Korean J. Chem. Eng., **28**(1), 143-148 (2011)
DOI: 10.1007/s11814-010-0397-y

Polarization characteristics and fuel utilization in anode-supported solid oxide fuel cell using three-dimensional simulation

Ji Won Hwang, Jeong Yong Lee, Dong Hyun Jo, Hyun Wook Jung†, and Sung Hyun Kim

Department of Chemical and Biological Engineering, Korea University, Seoul 136-713, Korea
(*Received 28 April 2010 • accepted 30 July 2010*)

Abstract−A three-dimensional numerical simulation for anode-supported tubular solid oxide fuel cell (SOFC), which is characterized by good electrical conductivity, has been carried out. Performance results by simulation are in good agreement with those by experiments, reported in [7]. Effect of various process conditions such as operating temperature, inlet velocity of fuel, and flow direction of inlet gases on the cell performance and fuel utilization has been further scrutinized. Polarization curve rises with increasing temperature of preheated gases and chamber, resulting from the incremented activity of catalysts within electrode. An effective way to reduce the temperature variation in the single cell with increasing current density has been sought, considering the temperature-dependent thermal expansion of materials. It has also been found that the fuel utilization is enhanced by increasing the cell length and operating temperature and lowering the inlet velocity of fuel.

Key words: Anode-supported SOFC, Fuel Utilization, Polarization Curve, Simulation, Cell Performance

INTRODUCTION

Technologies and applications for fuel cells have been enormously advanced with many researchers' efforts in both academia and industry. Among the several kinds of fuel cells, the solid oxide fuel cell (SOFC), which is conventionally operated at high temperature, has been widely explored as a promising energy source since this has salient features such as no need of noble metal catalysts and the direct usage of various fossil fuels in the reforming stage. SOFC generally consists of anode with NiO+YSZ (yttria-stabilized zirconia), cathode with LSM (strontium-doped lanthanium manganite)+ YSZ, and electrolyte with YSZ. Both electrodes which are porous for the favorable diffusion of gases are made of electrically conducting materials, whereas the electrolyte between both electrodes is non-conducting. SOFCs are classified into planar, tubular, and planar-tubular or anode-supported, cathode-supported, and electrolyte-supported, according to their own distinguishing characteristics. SOFC generates electricity by reactions of hydrogen and oxygen, as shown below. Hydrogen gas reacts with oxygen ion at the anode and loses its electrons. Then, electrons transfer to the cathode site for the reduction reaction through conducting wire.

Anode: $H_2+O^{2-} \rightarrow H_2O+2e^-$

Cathode: $\frac{1}{2}O_2+2e^- \rightarrow O^{2-}$

Many research groups have endeavored to develop numerical simulations for internal dynamics and performance of SOFCs as the efficient and reliable measurement tools in place of the elaborate and rather expensive experiments. For instance, Vayenas and Debenedetti [1] considered SOFC as chemical-electrocatalytic reactor. Hirano et al. [2] developed the non-isothermal 2-D model for (cathode-supported) tubular SOFC. 3-D models have been further exploited for (cathode-supported) tubular SOFC by many researchers [3,4]. Also, Li and Chyu [5] and Li and Suzuki [6] substantiated their 2-D model with experimental observations from the literature. However, there still remain unsolved theoretical issues on SOFCs, e.g., bundle or stack configuration, optimal strategy for current collection, sensitivity of SOFC systems, and arrangement of BOP (balance of plant) with fuel cells for high energy efficiency - via multi-dimensional simulations albeit in productive progress.

In this study, dynamics and performance of tubular SOFC have been investigated through 3-D calculations. Among the several kinds of SOFCs, anode-supported SOFC with thick anode substrate to mechanically support the electrolyte and cathode has been focused here because anode material has superior electrical conductivity and its enhanced thickness does not increase electrical resistivity. Polarization curves from the simulation have successfully corroborated experiments [7]. Also, the effect of several process conditions on the cell performance and fuel utilization has been systematically scrutinized.

NUMERICAL SCHEMES

1. Model and Numerical Simulation for SOFC

To evaluate the transport phenomena and electrochemical reaction in SOFC, FLUENT CFD software equipped with an SOFC module based on the finite volume method has been employed [8]. This comprises CFD-basic module for conservation equations of species, momentum, energy and electric potential field and SOFC sub-module for the electrochemical models such as Nernst voltage, current distribution and overpotentials at the electrolyte. The procedure for SOFC calculation is illustrated in Fig. 1. The computational domain and grids with 160,000 cells were constructed by GAMBIT, guaranteeing numerical convergence, as schematically depicted in Fig. 2. Some key equations are briefly explained hereafter.

†To whom correspondence should be addressed.
E-mail: hwjung@grtrkr.korea.ac.kr

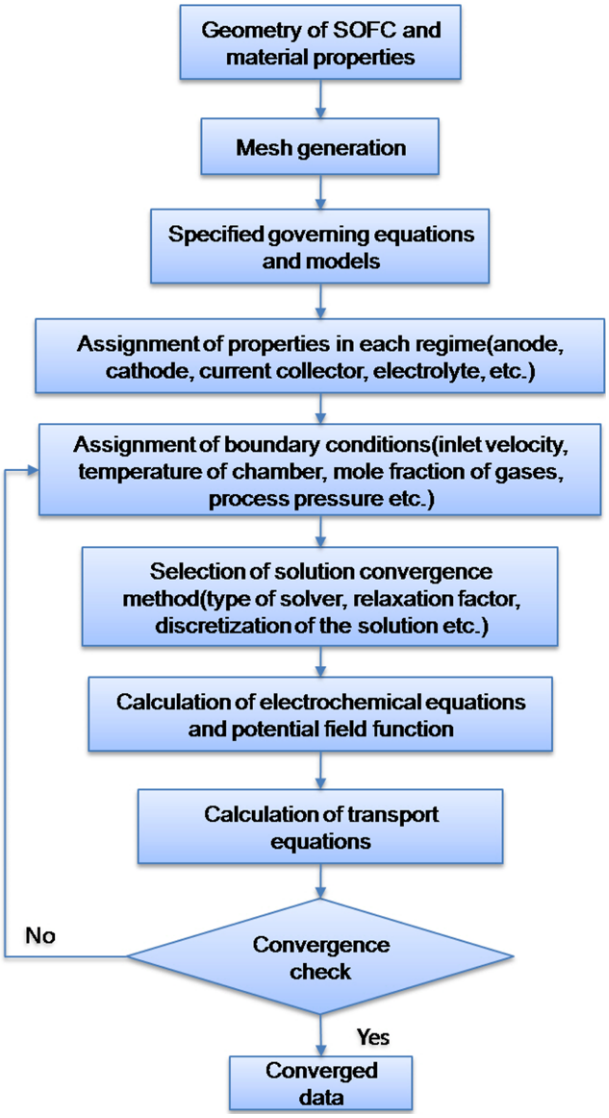

Fig. 1. Procedure for SOFC calculation.

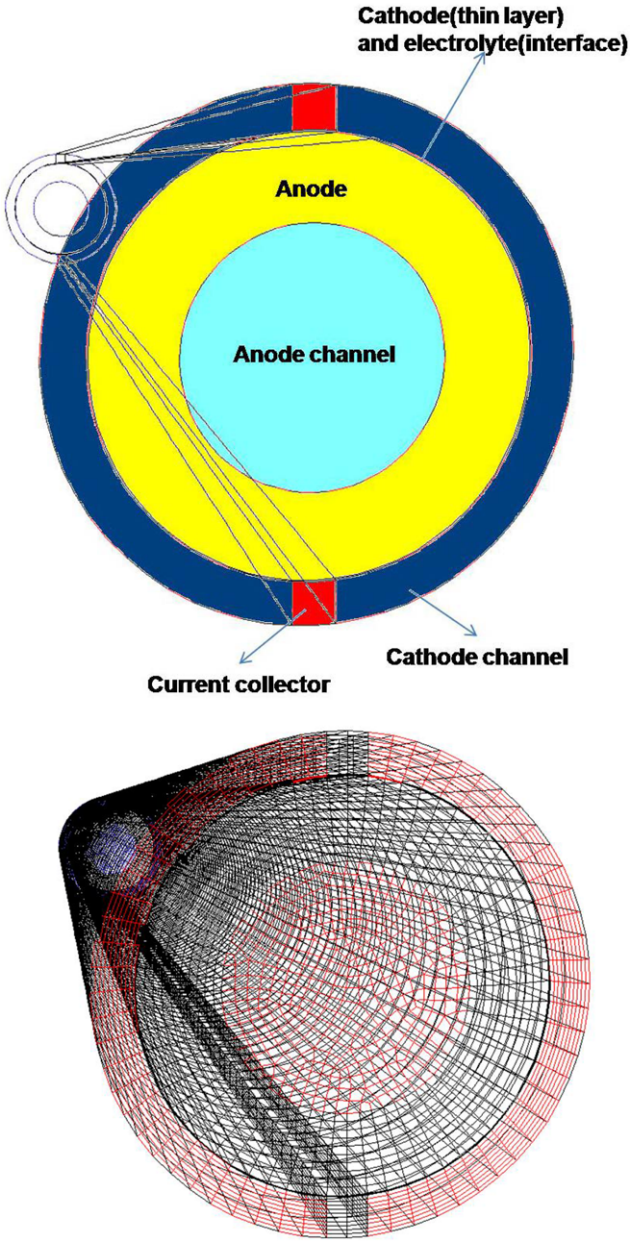

Fig. 2. Structure and mesh generation of the tubular SOFC.

2. Transport Equations

Transport equations to be applied in this study are briefly explained herewith [9].

2-1. Equation of Motion

$$\rho(\underline{v}\cdot\underline{\nabla}\underline{v}) = -\underline{\nabla}P + \underline{\nabla}\cdot[\mu(\underline{\nabla}\underline{v} + (\underline{\nabla}\underline{v})^{T})] + \underline{f} \quad (1)$$

where, ρ denotes the density of gas mixture, $\underline{v}$ the velocity vector, P the pressure, μ the viscosity of gas mixture, and $\underline{f}$ the external force. In anode and cathode channels, the above equation is incorporated to calculate the velocity distribution and pressure gradient. Fuel and air are regarded the ideal gas mixture because the system is operated under extremely high temperature of about 650-800 °C and atmospheric pressure. It will also be adequate to consider that the viscosity of gas mixture obeys the ideal gas mixing law as expressed below [10].

$$\mu_{mix}^{ig} = \sum_{i} x_i \mu_{pure\,i}^{ig} \quad (2)$$

where, x_i is mole fraction of pure species. The external force $\underline{f}$ such as gravitational force is neglected here.

2-2. Equation of Continuity

$$\text{Anode: } \underline{\nabla}\cdot(\rho\underline{v}) = S_{H_2} + S_{O^{2-}} + S_{H_2O} \quad (3)$$

$$\text{Cathode: } \underline{\nabla}\cdot(\rho\underline{v}) = S_{O_2} + S_{O^{2-}} \quad (4)$$

Continuity equations applied in gas channels balance with mass of gases. The velocity vector from the equation of motion is substituted and the mass source S's are calculated by the current density and stoichiometric coefficient of each species.

2-3. Equation of Energy

$$\underline{\nabla}\cdot(\underline{v}(\rho E + P)) = \underline{\nabla}\cdot\left(k_{eff}\underline{\nabla}T - \sum_{j} h_j \underline{J}_j + (\underline{\underline{\tau}}_{eff}\cdot\underline{v})\right) + Q_h \quad (5)$$

where k_{eff} represents the effective thermal conductivity, T the tem-

perature, h_j the enthalpy of the species, $\underline{\tau}_{eff}$ the effective shear stress tensor, Q_h the heat source by electrical resistance, and $\underline{J}$ the mass flux vector. E contains the internal, potential, and kinetic energies. Convective heat inside the cell balances with conductive heat, enthalpy change by reactions, viscous dissipative heat, and heat by electrical resistance, respectively. It is worth mentioning that the convective heat transfer is dominant in gas channels, compared with the conductive heat transfer; however, this can be neglected in electrodes because the gas velocity is not considered there.

2-4. Diffusion of Species

In both gas channels and electrodes, the mass diffusion by Fick's law should be implemented.

$$\underline{J}_i = -\rho D_{ij} \underline{\nabla} \omega_i \tag{6}$$

where, ω_i denotes mass fraction. The diffusivity D_{ij} of the air and fuel mixture must be modified to the effective diffusivity considering the porosity, ε and tortuosity, ξ of the porous electrode.

$$D_{ij,eff} = \frac{\varepsilon}{\xi} D_{ij} \tag{7}$$

3. Electrochemical Equations

The equation for an electric field is expressed in Laplacian form (Eq. (8)), based on the charge conservation $\underline{\nabla} \cdot \underline{i} = 0$ [11] and definition of the current density $\underline{i} = -\sigma \underline{\nabla} \phi$, where σ is the electrical conductivity of electrodes and ϕ the electrical potential.

$$\underline{\nabla} \cdot (\sigma \underline{\nabla} \phi) = 0 \tag{8}$$

The potential field must consider a potential jump employed between the two sides of the non-conductive wall to account for the effect of the electrochemistry. Also, several overpotentials, deteriorating cell performance from the ideal potential (ϕ_{ideal}), should be involved in estimating actual cell potential: ohmic overpotential (η_s) in the conductive solid regions (e.g., electrodes and current collector), ohmic overpotential at the electrolyte (η_{ele}), activation overpotentials at the anode ($\eta_{act,a}$) and the cathode ($\eta_{act,c}$). The potential jump from anode to cathode side can be described by overpotentials at the electrode (Eq. (9)). Therefore, the total cell potential is calculated from the potential jump between electrodes and the ohmic overpotential of the electrolyte (Eq. (10)).

$$\phi_{jump} = \phi_{ideal} - \eta_{ele} - \eta_{act,a} - \eta_{act,c} \tag{9}$$

$$\phi_{cell} = \phi_{jump} - \eta_s = \phi_{ideal} - (\eta_s + \eta_{ele} + \eta_{act,a} + \eta_{act,c}) \tag{10}$$

The ideal potential of the cell at equilibrium state is expressed by the Nernst equation [12].

$$\phi_{ideal} = \phi^0 + \frac{RT}{nF} \ln \prod_i p_i^{\nu_i} \tag{11}$$

where ϕ^0 denotes the potential at standard state, p_i the partial pressure of species i, ν_i the stoichiometric coefficient of reactants and products, and F the Faraday constant. Activation overpotential, the energy loss due to the slow electrochemical reaction in the electrode, is evaluated by Butler-Volmer equation which represents the net current by reaction with exchange current density, i_0, transfer coefficient, α, number of electrons, n, and activation overpotentials, $\eta_{act,a}$ and $\eta_{act,c}$.

$$\text{Anode: } i = i_{0,a} \left[e^{\frac{\alpha n F \eta_{act,a}}{RT}} - e^{\frac{-\alpha n F \eta_{act,a}}{RT}} \right] \tag{12}$$

$$\text{Cathode: } i = i_{0,c} \left[e^{\frac{\alpha n F \eta_{act,c}}{RT}} - e^{\frac{-\alpha n F \eta_{act,c}}{RT}} \right] \tag{13}$$

The exchange current density, i_0, in Eqs. (12) and (13) is closely related to the microstructural geometry of the electrode [13]. Due to the nonlinearity of the Butler-Volmer equation, activation overpotential should be solved by iterative Newton's method. Current density, i, is finally obtained by inserting the cell potential in Eq. (8). Detailed material properties and operating conditions for the simulation are listed in Tables 1 and 2.

RESULTS AND DISCCUSION

1. Model Validation

First, we tried to validate polarization data from simulation by

Table 1. Geometric and material properties

Properties	Value
Geometry	
Cell length (mm)	160
Thickness of anode (mm)	2
Thickness of cathode (μm)	50
Thickness of electrolyte (μm)	5
Anode	
Porosity	0.33
Tortuosity	4.5
Electrical conductivity (S/cm)	1500
Density (kg/m^3)	3030
Heat capacity (J/kg·K)	595.1
Heat conductivity (W/m·K)	11
Cathode	
Porosity	0.4
Tortuosity	4.5
Electrical conductivity (S/cm)	220
Density (kg/m^3)	4375
Heat capacity (J/kg·K)	567.5
Heat conductivity (W/m·K)	6.0
Electrolyte	
Density (kg/m^3)	5371
Heat capacity (J/kg·K)	585.2
Heat conductivity (W/m·K)	2.7
Current collector	
Density (kg/m^3)	8900
Heat capacity (J/kg·K)	446
Heat conductivity (W/m·K)	72

Table 2. Process and boundary conditions

Properties	Value
Anode channel	
Inlet velocity (m/s)	1.47
H_2/H_2O mass fraction	0.3/0.7
Cathode channel	
Inlet velocity (m/s)	3.92
N_2/O_2 mass fraction	0.7671/0.2329

comparing with experimental ones measured by Lee et al. [7]. The active length of the cell is 160 mm and the thicknesses of anode, cathode, and electrolyte are 2 mm, 50 μm and 5 μm, respectively. The experiment was carried out at 1,073 K operating temperature (i.e., furnace temperature) and inlet flow rates of humidified hydrogen and air were 2.5 L/min (1.47 m/s) and 6.7 L/min (3.92 m/s), respectively. It is noted that contact resistances between electrodes and current collectors were determined as best-fitted values: 10^{-7} ohm/m^2 at contact surface between anode and 10^{-6} ohm/m^2 at contact surface between cathode and current collector. As illustrated in Fig. 3, performance data from simulation quantitatively coincide with experimental observations. The reason why the simulation value of the open circuit voltage (OCV) is slightly lower than the experimental finding is due to the assumption of pre-heated fuels under the operating temperature. In experiments, fuels were not pre-heated to the operating temperature in the OCV stage with no reaction.

2. Effect of Operating Conditions on Cell Performance and Internal Temperature

One beneficial thing from the well-established numerical simulation is to properly expect the transport and electrochemical phenomena inside the single cell. The effect of operating temperature on the cell performance has been further scrutinized. This is one of key factors for manipulating overpotentials, readily altering the exchange current density, electric conductivity of electrodes, and ionic conductivity of electrolyte. It is obviously revealed that the increasing temperature decreases overpotentials, leading to the improved cell performance (Fig. 4).

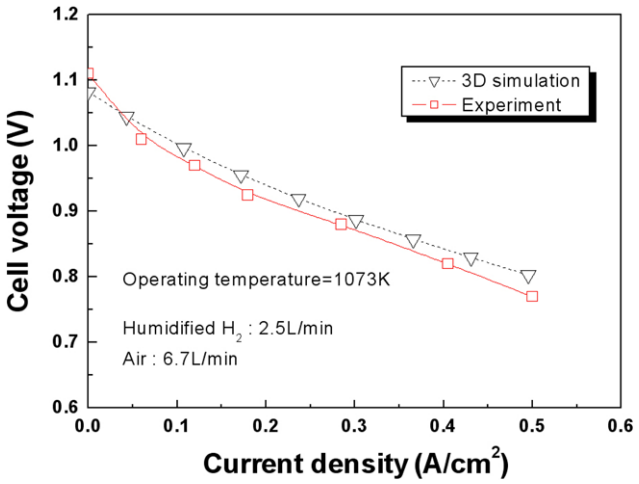

Fig. 3. Comparison of polarization curves from simulation and experiment.

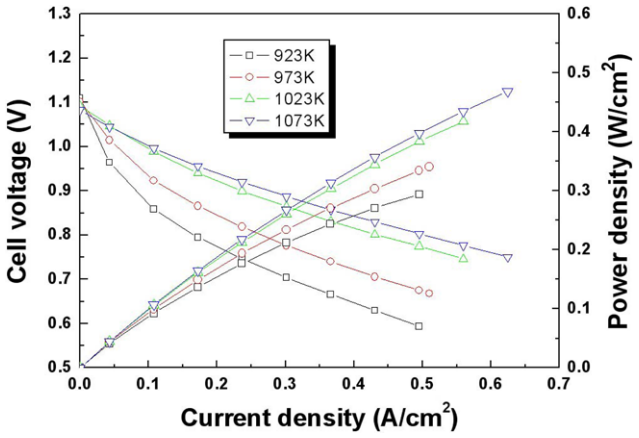

Fig. 4. Polarization curves and power density data at various temperatures.

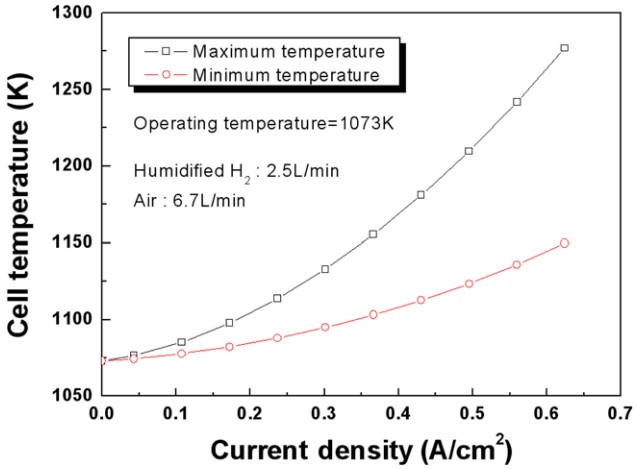

Fig. 5. Maximum and minimum temperatures in a single cell along with current density.

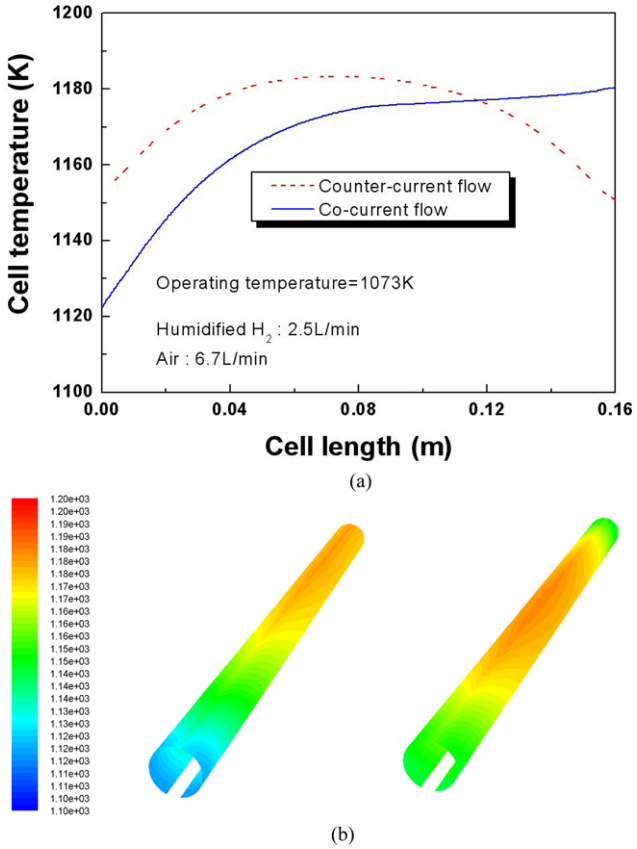

Fig. 6. Effect of fuel-flow direction on temperature distribution. (a) Averaged temperature profiles and (b) whole temperature contours for co-current (left) and counter-current (right).

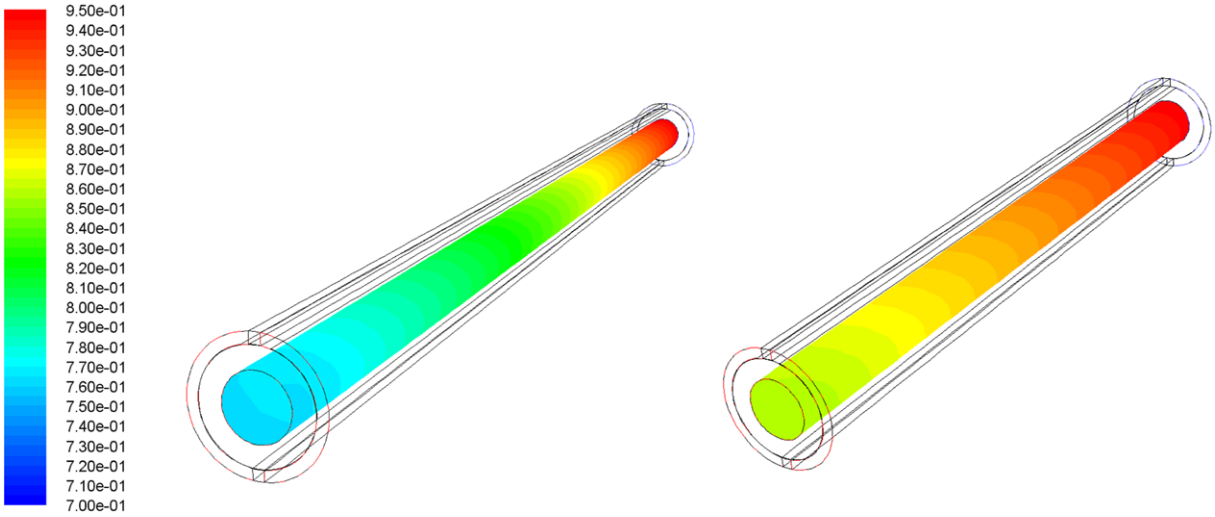

Fig. 7. Contours of fuel distribution in 160 mm (Max: 0.95, min: 0.762) and 80 mm (Max: 0.95, min: 0.855) cells at current density 0.366 A/cm^2 and operating temperature 1,073 K.

Maximum and minimum temperatures at the electrolyte inside the cell have been predicted with respect to the corresponding current density (Fig. 5) in the case that the operating temperature is kept constant. Temperature difference between maximum and minimum is raised as the current density increases. This might be caused by the reactive heat at the triple phase boundary (TPB) and dissipative heat by electric resistance at the electrode. It is practically crucial to control the temperature variation in the cell to protect the physical status of electrode and electrolyte made of inorganic ceramics from any crack due to the thermal expansion. Fig. 6 demonstrates that the temperature difference could be significantly reduced by changing the flow direction of gases. Co-current flow exhibits a temperature difference of 60 K through the whole cell length, whereas counter-current flow only gives a temperature difference of 30 K. This is based on the fact that temperature monotonically increases from inlet to outlet under co-current flow condition, but it has a maximum in the center region in the counter-current flow case.

3. Effect of Process Conditions on Fuel Utilization

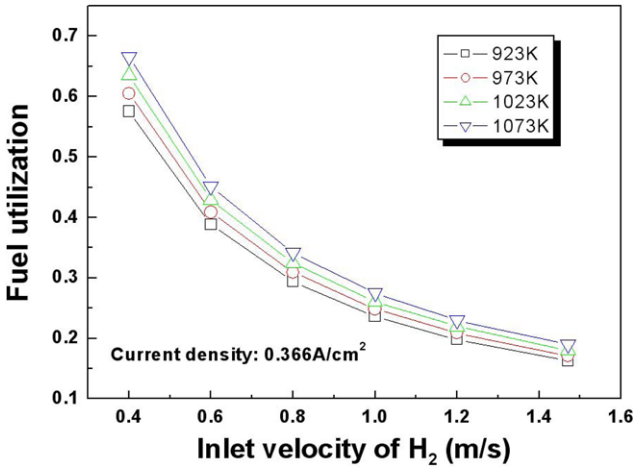

Fig. 8. Effect of inlet velocity of fuel and operating temperature on fuel utilization.

In fuel cell systems, it is also important to promote the fuel consumption in a single cell without additional recycling step for efficient energy saving. Fuel utilization is defined as the ratio of the amount of consumed fuel to the amount of supplied fuel. The effect of cell length on the fuel consumption was first examined. The cell with 160 mm length gives the fuel utilization of 0.188 and 80 mm cell provides the fuel utilization of 0.095 under the current density of 0.366 A/cm^2, temperature of 1,073 K and inlet velocity of fuel of 1.47 m/s (Fig. 7). The discrepancy of fuel utilization is intuitively ascribed to the residence time of fuel propagating whole cell. Thus, increasing the cell length is advantageous to improving the fuel efficiency. Fig. 8 shows the effect of inlet velocity of hydrogen on the fuel utilization at 1,073 K and current density of 0.366 A/cm^2. As in the previous case, the fast supply of fuel results in the decrease of fuel efficiency, owing to the insufficient reaction time. At the given current density (0.366 A/cm^2), the effect of operating temperature on fuel utilization is also shown in Fig. 8. As operating temperature increases, the fuel utilization is improved by the intensive reactions at anode and cathode.

CONCLUSIONS

Numerical simulations of anode-supported tubular SOFC have been conducted for investigating the cell performance and fuel utilization as well as internal dynamics. Validation of numerical results through the comparison with experimental observations published in [7] has been successfully confirmed. Furthermore, we have predicted how key process parameters such as operating temperature, cell geometry, amounts of fuel, etc., affect the cell performance and fuel utilization. Simulation methodology employed in this study will be helpful to further elucidate the bundle dynamics as well as the optimal single cell design and the best cell performance in SOFCs.

ACKNOWLEDGEMENTS

This study was supported by research grants from Korea Energy Management Cooperation (KEMCO) and Korea Institute of Energy

Technology Evaluation and Planning (KETEP).

NOMENCLATURE

$D_{ij,\,eff}$: effective diffusivity
E : internal, potential and kinetic energies
F : faraday constant
$\underline{J}$: mass flux vector
P : pressure
Q_h : heat source
R : gas constant
S : mass source
T : temperature
e : exponential constant
$\underline{f}$: external force vector
h : enthalpy
i : current density
i_0 : exchange current density
k_{eff} : effective thermal conductivity
n : number of electrons
p : partial pressure
$\underline{v}$: velocity of gas flow
x : mole fraction of pure species
α : transfer coefficient
ε : porosity
η_{ele} : ohmic overpotential by ionic conductivity at the electrolyte
η_{act} : activation overpotential
η_s : ohmic overpotential at the electrically conductive region
μ : gas viscosity
ξ : tortuosity
ρ : density of gas mixture
σ : electrical conductivity
$\underline{\tau}_{eff}$: effective shear stress tensor
ϕ : electrical potential
ϕ_{jump} : potential jump between the electrodes
ϕ_{ideal} : nernst potential
ω : mass fraction

Subscript
a : anode
c : cathode
i : species i
j : species j

Superscript
ν : stoichiometric coefficient
0 : standard state (25 °C, 1 atm)

REFERENCES

1. C. G. Vayenas and P. G. Debenedetti, *Chem. Eng. Sci.*, **38**, 1817 (1983).
2. A. Hirano, M. Suzuki and M. Ippommatsu, *J. Electrochem. Soc.*, **139**, 2744 (1992).
3. N. F. Bessette II, W. J. Wepfer and J. Winnick, *J. Electrochem. Soc.*, **142**, 3792 (1995).
4. J. R. Ferguson, J. M. Fiard and R. Herbin, *J. Power Sources*, **58**, 109 (1996).
5. P.-W. Li and M. K. Chyu, *J. Power Sources*, **123**, 487 (2003).
6. P.-W. Li and K. Suzuki, *J. Electrochem. Soc.*, **151**, A548 (2004).
7. S. B. Lee, T. H. Lim, R. H. Song, D. R. Shin and S. K. Dong, *Intern. J. Hydrogen Energy*, **33**, 2330 (2008).
8. Fuel Cell Modules Manual: ANSYS Group (http://www.fluent.com).
9. R. B. Bird, W. E. Stewart and E. N. Lightfoot, *Transport phenomena*, *2nd Ed.*, John Wiley & Sons, New York (2002).
10. J. P. O'Connell and J. M. Haile, *Thermodynamics: Fundamentals for applications*, Cambridge University Press, New York (2005).
11. A. Bettini, *Introduction to elementary particle physics*, Cambridge University Press, New York (2008).
12. J. Larminie and A. Dicks, *Fuel cell systems explained*, *2nd Ed.*, John Wiley & Sons, Chichester (2003).
13. M. Ni, M. K. H. Leung and D. Y. C. Leung, *Energy Convers. Manage.*, **48**, 1525 (2007).